IOP PUBLISHING JOURNAL OF PHYSICS D: APPLIED PHYSICS

J. Phys. D: Appl. Phys. **41** (2008) 015503 (5pp) doi:10.1088/0022-3727/41/1/015503

Driven intrinsic localized modes in a coupled pendulum array

R Basu Thakur[1], **L Q English**[1] **and A J Sievers**[2]

[1] Department of Physics & Astronomy, Dickinson College, Carlisle, PA 17013, USA
[2] Laboratory of Atomic and Solid State Physics, Cornell University, Ithaca, NY 14853, USA

Received 18 October 2007, in final form 22 November 2007
Published 19 December 2007
Online at stacks.iop.org/JPhysD/41/015503

Abstract
Intrinsic localized modes (ILMs), also called discrete breathers, are directly generated via modulational instability in an array of coupled pendulums. These ILMs can be stabilized over a range of driver frequencies and amplitudes. They are characterized by a π-phase difference between their centre and wings. At higher driver frequencies, these ILMs are observed to disintegrate via a pulsating instability, and the mechanism of this breather instability is investigated.

1. Introduction

Intrinsic localized modes (ILMs) are spatially localized, time-periodic excitations in nonlinear lattices analogous to solitons but sensitive to the lattice discreteness due to their extremely sharp localization. The ILM, or discrete breather, has become a very well-studied excitation in a wide variety of physical systems and has been firmly established as a conceptual entity on par with the soliton.

Initial studies of ILMs excluded damping or driving-key features from an experimental perspective. Later, analytical and numerical treatments found that the addition of a driver could modify the undriven ILM solutions in non-trivial ways [1–3]. Analytically, perhaps two of the most prominent models for which localized solutions have been demonstrated are the nonlinear Schroedinger equation and the sine-Gordon equation, both of which have proved relevant in the study of mechanical solitons [4]. Both equations have been analysed with the addition of a driving term [5–7], but both are rooted in the continuum approximation.

In previous experiments on coupled pendulum arrays, a vertical driver excited the pendulums parametrically at around twice the natural resonance frequency [8–10]. In these studies, the particular coupling between pendulums introduced large inter-site anharmonicity. In this paper, we examine a pendulum array with harmonic coupling and horizontal, sinusoidal driving. We observe modulational instability (MI) of the uniform mode which at longer times makes possible the formation of stable ILMs locked to the driver. We characterize these driven ILMs in terms of their spatial profiles for different driving frequencies and amplitudes. Finally, we examine an interesting pulsating instability of the ILM at higher driver frequencies and offer a possible mechanism for this instability [11].

2. Experimental details

The pendulum array is schematically shown in figure 1. The array consists of 15 pendulums connected by springs which couple them torsionally. Each pendulum comprises a brass base piece near the suspension point, a threaded rod screwed vertically into the base and a brass disc attached to the bottom end of the threaded rod which serves as the weight. The pendulums are suspended on taut piano wire of 0.041 in. diameter which runs through the base of each pendulum and is held up by the outer frame. Springs of diameter 0.4 in. slip tightly over sleeves at each end of the base pieces and are then glued onto that sleeve for additional support. No slippage of the spring with respect to the pendulum base was ever observed. The first and last pendulums are coupled only to their one neighbour, the other end resting against a spacer piece to keep it at a fixed distance from the frame; this results in open boundary conditions. Due to the use of a threaded rod, the effective length of the pendulums is adjustable. The weights are calibrated 5 g discs.

Figure 2 illustrates the larger experimental setup. The pendulum array (i) rests securely on a frame (ii) with low-friction wheels (iii). A high-torque electric motor (90 V, 190 W) is attached to the cart via a crankshaft (iv) and moves it horizontally at a constant but voltage-adjustable frequency. This sinusoidal horizontal motion of the pendulum platform translates into a driving torque on the pendulums.

 © 2008 IOP Publishing Ltd Printed in the UK

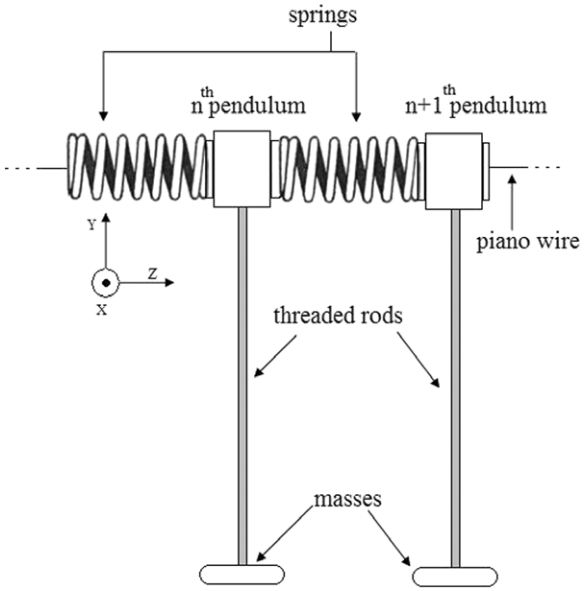


Figure 1. The experimental system: pendulums connected by torsional springs.

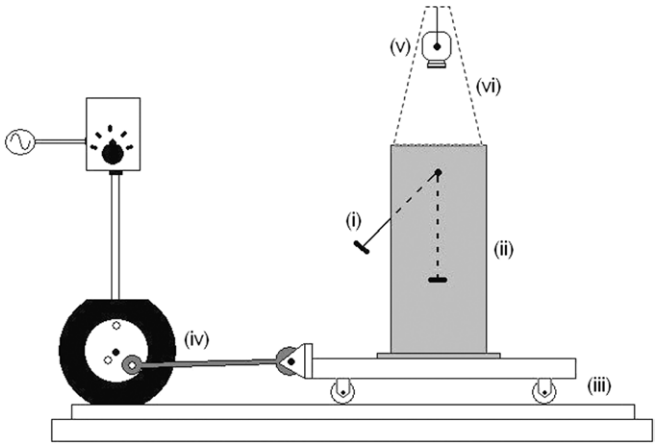


Figure 2. The experimental setup.

The frequency and amplitude of the driver is independently determined using a Vernier linear motion sensor tracking the pendulum platform. The pendulum motion was captured by an overhead wide-angle web-cam (v) which was fixed to the frame of the pendulum array (vi). Pendulum coordinates can then be extracted frame by frame via video analysis software (Logger Pro, Vernier).

Four main torques act on each pendulum: gravitational, spring, damping torques, as well as a centrifugal driving torque by virtue of the non-inertial reference frame. Thus, the equation of motion of the nth pendulum takes the form,

$$\frac{\mathrm{d}^2\theta_n}{\mathrm{d}t^2} + \omega_0^2 \sin(\theta_n) - \left(\frac{c}{a}\right)^2 [\theta_{n+1} + \theta_{n-1} - 2\theta_n] + \eta \cos(\omega_d t)\cos(\theta_n) + \gamma \frac{\mathrm{d}\theta_n}{\mathrm{d}t} = 0. \quad (1)$$

The second term in equation (1) is due to the gravitational restoring torque, the third term due to the nearest neighbour spring coupling, the fourth incorporates the driver and the last term accounts for velocity-dependent friction. The spring restoring force was confirmed experimentally to be quite linear up to an angle difference of 90°, so that the only source of nonlinearity is in the gravitational term. Thus, in contrast to the micromechanical cantilever arrays [12, 13], the nonlinearity is strictly on-site. The constants in equation (1) can be expressed in terms of measurable properties of our experimental system (see appendix):

$$\omega_0^2 = \frac{1}{I}\left(mg\frac{L}{2} + MgL\right),$$
$$\eta = \frac{A\omega_\mathrm{d}^2}{I}\left(\frac{mL}{2} + ML\right), \quad (2)$$
$$I = ML^2 + \frac{1}{3}mL^2,$$

where m is the mass of the rod, M that of the disc and A the driving amplitude. The coupling- and friction constants, c and γ, can be measured directly. The Q-factor of the system is around 120.

Equation (1) is similar to the discrete sine-Gordon equation. The driver's torque, however, introduces a cosine term (instead of the sine for parametric driving [8]), and there is a velocity-dependent damping term.

Equation (1), without the last two terms and in the harmonic limit, results in a linear plane-wave dispersion curve of the form,

$$\omega(k) = \sqrt{\omega_0^2 + 2\left(\frac{c}{a}\right)^2 (1 - \cos(ka))}, \quad (3)$$

with ω_0 as given in equation (2). Inserting realistic experimental values, we compute the following important frequencies: $\omega_0 = 6.95\,\mathrm{rad\,s^{-1}}$, $\omega_{ZB} = 7.6\,\mathrm{rad\,s^{-1}}$. The driver frequency, ω_d, is in the range of 5.3–6.3 $\mathrm{rad\,s^{-1}}$, ensuring that no ILM overtones lie within the linear spectrum.

3. Results and discussion

Figure 3 illustrates one pathway to stable driven ILMs, namely the MI of the uniform pendulum mode. The traces depict the positions of the 15 pendulums at the instant the central pendulum reaches its turning point. The first trace in figure 3(a) shows the pendulums soon after the driver has been turned on. The driver frequency is set to 99% of the linear resonance frequency ($\omega_\mathrm{d} = 6.85\,\mathrm{rad\,s^{-1}}$). The subsequent traces in figure 3(a) show the turning points of the pendulums at later times as they acquire more energy from the driver. In traces 3 and 4, an emerging spatial variation can already be observed. This spatial variation quickly escalates with time, as seen in figure 3(b). Traces 5–7 show the position of the pendulum chain at three successive periods of the centre pendulum. In trace 7 we see that three pendulums (including the centre one) are now out of phase relative to the rest of the chain. The times associated with each trace in order are 0.33, 2.3, 4.2, 6.2, 8.3, 9.4 and 10.6 s.

The MI essentially amplifies the noise sufficiently for the system to eventually settle into one or more ILMs [3]. It

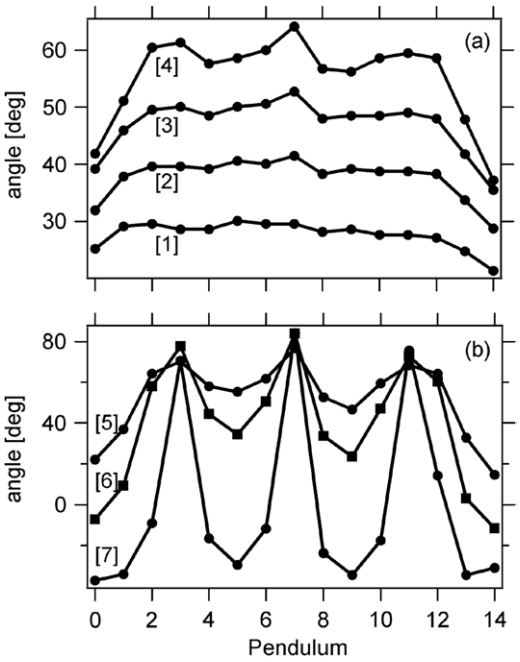


Figure 3. The MI develops as the pendulums are driven first at resonance (*a*) and then below resonance (*b*).

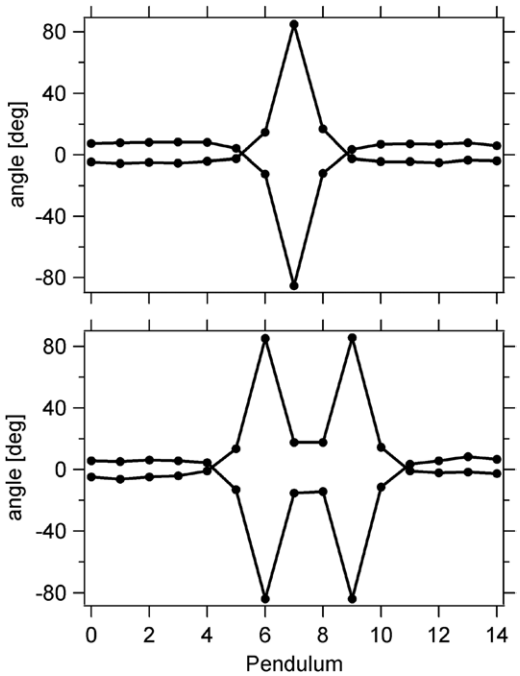


Figure 4. The long-time profile of driven ILMs. Note that in both cases, the wings perform small out-of-phase oscillations. (*a*) One ILM at the centre of the chain (pendulum 7). (*b*) Two in-phase ILMs next to one another.

should be emphasized that in order to produce an ILM using the MI, it is essential that the frequency be decreased during the run. We have found experimentally that it is best to start lowering the frequency at the time the spatial variation first becomes noticeable, i.e. somewhere between traces 3 and 4 of figure 3(*a*). In this run, the frequency was first set to resonance and then lowered within 3 s by about 10% to $\omega_d = 6.1\,\mathrm{rad\,s^{-1}}$. In this way, a stable driven ILM was generated in this particular run centred at pendulum 7. The location of the ILM within the chain and even the number of ILMs produced cannot be predicted *a priori*, and is different from run to run, as expected for a uniform system of discrete nonlinear elements.

Figure 4(*a*) shows a typical profile of a driven ILM produced via the MI at long times. Evidently, the ILM is localized to about three pendulums. Interestingly, the wings are 180° out of phase with respect to the centre of the ILM. Subsequent comparison with the driver phase reveals that the centre is out of phase with the driver. In figure 4(*b*), another possible stable ILM solution is depicted. Here two ILMs oscillating in phase with one another (but out of phase with the driver) are produced via MI; the ILM peaks are separated only by two pendulums.

Theoretical studies [1–3] have predicted the existence of ILMs with a 180° phase difference between the centre and the wings. This creates what [1] calls a 'phase-domain wall' of just one or two pendulums in width. In systems with soft nonlinearity, the low-amplitude wings are in phase with the driver (as the driver frequency is below the low-amplitude resonance frequency), and the ILM centre is out of phase. A second type of ILM is also predicted where both the centre and the wings are in phase with the driver. We have not been able to stabilize this solution experimentally over long times.

Once a stable solution of a driven ILM is obtained experimentally, one can slowly vary the frequency of the driver to see what effect this has on the ILM profile. The results for two driver amplitudes, 7.5 (filled circles) and 2.5 mm (open squares), are illustrated in figure 5. Note that the x-axis measures the frequency ratio squared. It is evident that stable ILM solutions can be obtained over a limited range of frequencies. When lowering the frequency gradually, the locked ILM adjusts by increasing its amplitude and becoming narrower as it moves away from the plane-wave spectrum. Eventually, the ILM simply decouples from the driver and proceeds to damp out as if no driver were present. This happens sooner for lower driver amplitudes, as depicted in the figure.

At the higher limit, the driven ILMs are observed to undergo low-frequency oscillations in amplitude (and width) or pulsations. Above a certain frequency threshold, these pulsations grow in time and eventually destroy the ILM. For low driver amplitudes, this threshold is higher, allowing one to observe broader ILMs. Remarkably, when the results obtained from the two driver amplitudes are superimposed as in figure 5, they appear to fall on the same general curve. Perhaps not surprisingly, the data points for the driven ILMs deviate from the solutions to the continuous sine-Gordon equation (dashed line) [4], especially for lower frequencies, i.e. sharper ILMs.

When the driver frequency crosses a threshold, unstable ILM pulsations set in. For instance, at $\omega_d = 6.52\,\mathrm{rad\,s^{-1}}$, corresponding to a frequency ratio squared of 0.91 and amplitude 2.5 mm (see squares figure 5), very long-lasting ILM pulsations can be observed. The pulsation period is about 20 times longer than the ILM period, and here the ILM pulsation persists for about 18 min gradually growing in modulation amplitude. Just before disintegration, the ILM often hops to a neighbouring site temporarily, and soon full-blown chaotic dynamics ensues.

To highlight the nature of this instability, we now change the boundary conditions to fixed. The driver amplitude is raised to 5.5 mm and the frequency is set above the instability threshold (corresponding to this amplitude) to 6.46 rad s^{-1}. Figure 6(*a*) tracks the angle at the turning point, or the maximum angle, for three different pendulums. In the bottom, the diamonds represent the centre pendulum (pendulum 8), and in the top the filled and open circles represent pendulums 4 and 5, respectively. Thus, the upper half of the figure depicts pendulums in the wings of the ILM and the lower half depicts the central pendulum. Note that since none of the markers are at the same time, only amplitude but no phase relationship between the pendulums can be inferred from this figure alone. However, the wings and the centre tend to be out of phase except around the times of the minimum wing amplitude (line labelled (3) in figure 6(*a*)).

From the diamonds, it is apparent that the amplitude of the ILM is modulated and that this modulation grows with time. The wings undergo the same modulation, but figure 6(*a*) demonstrates that the two modulations are not π out of phase, as might be expected for a simple pulsating ILM alternately sharpening and broadening. The situation here is more complex, as illustrated by the profiles shown in figures 6(*b*)–(*d*).

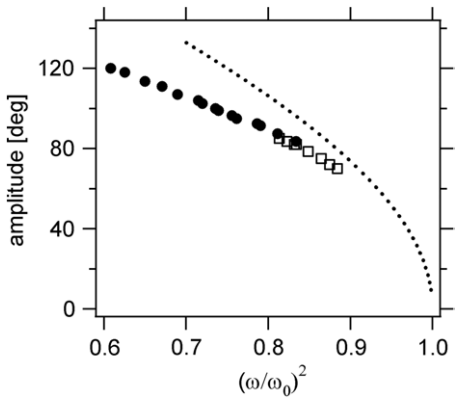


Figure 5. The amplitude in degrees of the central pendulum of the driven ILM as a function of the driver (and ILM) frequency. The frequency interval over which ILMs can be produced depends on the driver amplitude. Filled circles represent an amplitude of 7.5, open squares 2.5 mm.

Figure 6(*b*) depicts the position of all pendulums at the time of the maximum amplitude of the central pendulum; in figure 6(*a*) this time is represented by the line labelled (1). We see a typical ILM profile with the wings out of phase against the centre. Note, however, that in figure 6(*a*) the wings are already gaining amplitude at that time. A while later their amplitude has attained the local maximum while the ILM centre is approaching its minimum amplitude, see the second vertical line (2) in (*a*). For this time, the profile is depicted in figure 6(*c*). The solid line depicts the actual pendulum positions, whereas for later comparison the dotted line depicts a pure sine wave, the third allowed standing wave in the system (see discussion below). Finally, figure 6(*d*) shows the pendulum profile at the time of the minimum wing amplitude; see vertical line (3). Most of the pendulums momentarily move in phase at this time.

From figure 6(*c*) it is evident that a particular standing-wave mode is momentarily excited (see the dotted line). The following possible interpretation of the breather instability mechanism emerges. Since undriven ILMs in the sine-Gorden system are predicted to be stable [14], it is the addition of the driver that creates this instability. Since driven ILMs always have motion in their wings, we can think of the driven ILM as composed of a central localized peak superimposed on a uniform-mode background [11]. As the driver frequency is raised, this background component increases in amplitude because the driver gets closer to the resonance frequency. The presence of a non-negligible uniform mode of wavenumber k_1, where $k_n = (\pi/L)n$, renormalizes the frequencies of all the other plane-wave modes. In particular, it pulls down the other

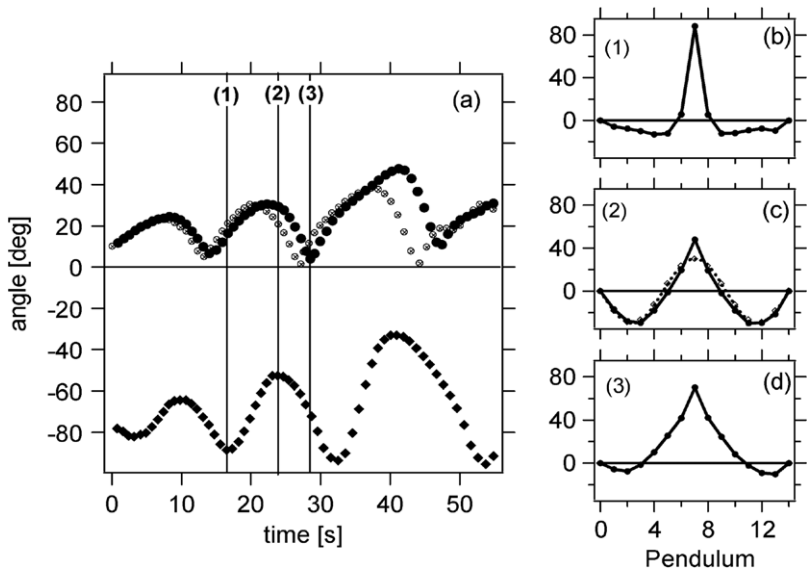


Figure 6. (*a*) ILM instability at higher driver frequencies. The lower trace shows the maximum angle attained by the centre pendulum in each period; the two upper traces are for two pendulums in the wings. (*b*)–(*d*) The ILM profiles at the select times (1), (2) and (3) also shown in (*a*).

long-wavelength modes, k_2 and k_3. For instance, if we expand the sine in equation (1) to second order, it is straightforward to show that in the presence of a uniform mode of amplitude θ_0, perturbations ε_n obey the following equation:

$$\ddot{\varepsilon}_n + \omega_0^2 \left(1 - \frac{1}{2}\theta_{k=0}^2(t)\right)\varepsilon_n - \left(\frac{c}{a}\right)^2 (\varepsilon_{n+1} + \varepsilon_{n-1} - 2\varepsilon_n) = 0.$$

Thus, the original low-amplitude plane-wave frequencies of equation (3) are approximately modified to

$$\omega(k) \approx \sqrt{\omega_0^2 \left(1 - \frac{1}{4}\theta_0^2\right) + 2\left(\frac{c}{a}\right)^2 (1 - \cos(ka))}. \qquad (4)$$

The important standing-wave mode to consider is k_3, since it shares the symmetry of the driven ILM. Therefore, in contrast to k_2, we expect that the driven ILM and a degenerate k_3-mode should be able to exchange energy easily. Thus, when their frequencies are first matched, the ILM (both components) transfer energy to the k_3-mode. Since the ILM amplitude is lowered, the excited standing wave (k_3-mode) moves back up in frequency. As its phase relationship to the ILM changes, it briefly transfers energy back to the ILM and driver, before the energy transfer stops. Subsequently, the driver can build up the ILM once more.

Incidentally, this interpretation explains why a lower-amplitude driver pushes the instability region to higher driver frequencies, as shown in figure 5. A lower-amplitude driver simply must be closer in frequency to ω_0 in order to excite the wings to the same amplitude.

In short, the nonlinear coupling and decoupling between ILM and third allowed plane-wave mode, as well as both modes' interaction with the driver, give rise to this pulsating breather instability. More detailed analytical work is necessary to fully characterize this phenomenon.

Acknowledgment

This research was supported by an award by the Research Corporation. We thank Richard Lindsey for much help in constructing the apparatus.

Appendix

The gravitational restoring torque comes in two parts because we have a rod of non-negligible mass as well as an end-mass. The magnitude of this torque is

$$\left(MgL + mg\frac{L}{2}\right)\sin(\theta).$$

When dividing by the moment of inertia (which also comes in two parts), we obtain the frequency squared, as in equation (2).

The driving torque comes about due to the horizontal motion of the pendulum array by an outside motor. To obtain the expression for the driving torque, we stay within the non-inertial reference frame of the pendulums. In this frame, the fictitious centrifugal force acts on each pendulum, namely, $F_c = -ma_{base}$. This force acts on the rod at its centre of mass in a horizontal direction, and it thus gives rise to the torque, $\tau_d = A\omega_d^2 \cos(\omega_d t)\left(\frac{mL}{2}\right)\cos(\theta_n)$. For the end-mass, the torque expression is almost identical, except that the force acts at a distance L from the pivot. Thus, we obtain the expression for η in equation (2).

References

[1] Roessler T and Page J B 1995 *Phys. Lett.* A **204** 418
[2] Roessler T and Page J B 1996 *Physica* B **219–220** 387
[3] Maniadis P and Flach S 2006 *Europhys. Lett.* **74** 452
[4] Remoissenet M 1999 *Waves Called Solitons* (3rd edn) (Berlin: Springer)
[5] Bishop A R *et al* 1983 *Phys. Rev. Lett.* **50** 1095
[6] Lomdahl P S and Samuelsen M R 1985 *Phys. Rev.* A **34** 664
[7] Forinash K and Willis C R 2001 *Physica* D **149** 95
[8] Chen W Z 1994 *Phys. Rev.* B **49** 15063
[9] Lou S Y and Huang G X 1995 *Mod. Phys. Lett.* B **9** 1231
[10] Lou S Y *et al* 1996 *Mod. Phys. Lett.* B **10** 11
[11] Mazor A and Bishop A R 1987 *Physica* D **27** 269
[12] Sato M *et al* 2003 *Chaos* **13** 702
[13] Sato M, Hubbard B E and Sievers A J 2006 *Rev. Mod. Phys.* **78** 137
[14] Marin J L, Aubry S and Floria L M 1998 *Physica* D **113** 283